Classification of Lung Glandular cells for early detection of Cancer using Multiple Color Spaces and Scale Space Catastrophe Features

D. Venkataraman[1], Dr.J.Suganthi[2], Sajith Kecheril S[3], Dr. K.Sujathan[4]

[1.] Research Scholar, Department of CSE, Amrita Viswha Vidyapeetham, Ettimadai, Coimbatore Tamilnadu, India-641112. d_venkat@cb.amrita.edu
[2.] Professor & Head, Department of Computer Science and Engineering, Hindusthan College of Engineering and Technology, Coimbatore, Tamilnadu, India-641 032.

[3.] Assistant Professor, Department of CSE, Amrita Viswha Vidyapeetham, Amritapuri
[4] Regional Cancer Center, Dept of Pathaology, Thiruvanathapuram, India

Abstract: One of the biggest challenges the world face today is the mortality due to Cancer. One in four of all diagnosed cancers involve the lung cancer. The lung cancer remains the most common cancer-related cause of death both in developed and developing countries due to inhaling cancer-causing substance such as tobacco**.** Screening test help doctors to find and detect cancer at early stages. Several methods such as MRI, chest-X rays, CT Scan, etc., are available for screening tests. For developing countries, the cost involved for early detection with the available methods is not affordable. This paper presents a novel low cost method to detect and classify lung glandular cells as benign or malignant (Cancer cells) using conventional pap stained sputum cytology images. The microscopic sputum images are preprocessed and analysis is restricted to cellular regions. For segmentation we use multiple color spaces and clustering algorithms: K-Means and Fuzzy C-Means. Scale Space based Catastrophe points are used as features and are classified using Support Vector Machine (SVM). We successfully classified the glandular cells as benign or malignant cells with an accuracy of 78.61%.
[D. Venkataraman, J. Suganthi, Sajith Kecheril S, K. Sujathan. **Classification of Lung Glandular cells for early detection of Cancer using Multiple Color Spaces and Scale Space Catastrophe Features.** *Life Sci J* 2013;10(2):2971-2980] (ISSN:1097-8135). http://www.lifesciencesite.com. 411

Keywords: Fuzzy C-means, K-means, Color space, Scale space, Catastrophe theory, Deep structure, Feature extraction, SVM

1. Introduction

In developed and developing countries, lung cancer is a major threat to mankind. The main reason for the highest mortality, due to lung cancer is because of non availability of pre-screening system which can analyze the cancer cells at early stages. The task of screening with manual system available currently is difficult to process, involves more cost and is more time consuming. This motivated us to develop a new system which will automatically screen for malignancy in an affordable way which will increase the survival rate of lung cancer patients [44].

For prescreening, methods like bronchoscopy, CT scan and Sputum Cytology image are used . Out of these entire methods, sputum cytology images are best suited for prescreening because of noninvasive nature and cost effectiveness. Care was taken in producing good results at all stages, right from slide preparation to sputum cytology image and segmentation.

Segmentation is another important process which is very difficult in medical image processing. In our work, we have given a novel approach towards the segmentation of nuclear region of lung glandular cells in the given sputum cytology images. Various methods given by various authors for segmentation, such as morphological operations for segmentation, iterative methods, Hopfield Neural Network (HNN) on RGB and HSV color spaces to extract adenocarcinoma nuclei of lung, thresholding method for segmentation on grayscale images [1 – 7] is known from the literature.

For Multiple Color Spaces, Meas-Yedid et. al. [8] used Markov Random Field (MRF) clustering on RGB color space, Begelman et. al. [9] used fuzzy logic on CIELAB color space, Hu et. al. [10] used a variant of active contour on grayscale image, Phukpattaranont et. al. [11] applied neural network on RGB image for segmentation. Ko et. al. [12] used adaptive window based on local contrast on grayscale image, Palacios et. al. [13] used discrete wavelet transform and K-means clustering on HSV, LUV and YIQ color spaces. Taher et. al. [14] used HNN and FCM to segment lung cells on RGB image, Plissiti et. al. [15] used grayscale morphological reconstruction and connected regional minima along with FCM and SVM to detect nuclei in pap smear images. Wang et. al. [16] applied graph cut followed by active contour for nuclear segmentation. In RGB color space the color intensity values are highly correlated so in order

to extract valuable information it has to be decorrelated. So various authors have used different color spaces for information retrieval Huang et. al. [17], Chen et. al. [18], Zhao et. al. [19], Yuzheng et. al. [20], Anari et. al. [21] used HSV color space for segmentation. Combination of color spaces [22-28] also yielded good results. Unsupervised learning of K-means clustering [29] and Fuzzy C-means [15] were used for cell segmentation.

For feature extraction, we used Scale space theory [36] that analyse objects at different scales. Normally the nuclear feature extraction techniques are divided into morphometric, densitometric, textural and structural features [43]. These features vary for benign and malignant cells greatly. Malignant cells are characterized by the non uniform distribution of chromatin in nucleus which can be detected by textural and structural analysis. For feature extraction we used catastrophe points which is the major contribution of our work and then we used that feature for classification of glandular cells as benign or malignant using SVM [15, 31, 45, 46].

Outline of the paper: In section 2, we detail the imaging system used to capture the cell samples, and the resulting Data set. In section 3, the proposed architecture of the system is discussed along with various clustering techniques, multiple color space conversion used for segmentation and feature selection using scale spaces are discussed. Section 4, details the results and discussion of our work. We conclude with conclusion and future directions of our work in sections 5.

2. Data Set

The sputum cytology images used in this work were provided by Pathology department, Regional Cancer Center Thiruvananthapuram, India. The nature of cells was confirmed by expert cytopathologist. The images were captured by using a trinocular microscope fitted with a digital camera. The images were captured at 40X magnification level. The images are of 24 bit color depth with a spacial resolution of 3264x2448 pixels. The pap stained sputum samples are digitized using a digital microscope. The staining of the cellular materials varies widely in conventional pap staining. Normally the staining color varies from slide to slide and depends on various parameters like batch of stain prepared, age of cell, type of cell and also depends on the person preparing the slide. In this work we have used 1038 cell images which are cropped from the input sputum cytology images. Input cytology image is shown in the Figure 1.

3. The proposed system Architecture

The system architecture for the proposed method to analyze the sputum cytology cells is shown in Figure. 2. It includes preprocessing and segmentation of Pap stained sputum cytology images followed by feature extraction and classification of cell nuclei.

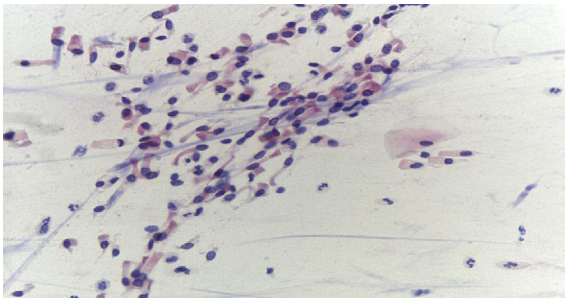

Figure 1. Input sputum cytology image provided by RCC, Thiruvananthapuram

Figure 2: Block diagram of the proposed system

3.1 Input Image

The sputum samples taken by cytotechnologists are preserved so that the cellularity of the nuclei is not lost. Then slides are prepared and stained using Pap stain. This is a differential stain in which the nuclear and cytoplasmic regions are stained in different colors. Nuclei region being more with dense materials and so will absorb more stain and appear much darker in color. The stained slide is placed under a trinocular light microscope and images are taken. The digital camera produces a high resolution image of 8 mega pixel (3264 X 2448) size. The slides are magnified at 40 X zoom level and images are taken. The images are stored on the workstation in 24 bit RGB color format. Images of both malignant and benign slides are taken. The classification of the slides as benign and malignant is done by experienced cytopathologists.

3.2 Pre Processing

The nuclei regions present in the image appears as dark blobs due to the absorption of stain in comparatively higher level than the cytoplasmic regions. By finding the local minima of the blobs the location of nuclei can be obtained. The high resolution input image is very difficult to process as such, so in this stage the image is down sized to $1/8^{th}$ of the original size (408X306). Local minima are found on the smoothed version of the image using Blom's method as used by Kuijper et al [33]. Once the local minima are identified, the coordinate in the resized image are mapped on to the original image. This is done by multiplying the x and y coordinate values by 8. Thus on the actual image coordinate a

128 X 128 sized image region is cropped out and is stored. The image may contain region without cellular material i.e., background regions. This has to be eliminated for further analysis. For this the average intensity value of the cropped region is calculated; if the value rises above 200 it is assumed to be background since nuclear regions being darkly stained will have a low average intensity only. The sputum cytology images are infiltrated by patches of mucus which also absorbs the stain. One more condition is given to filter out such regions. The standard deviation of the extracted region is calculated. If it is above 30 then there is an adequate distribution of dark and bright patches are present which is typical of nuclear region. All the cropped patches are saved. The sputum sample contains a lot of artifacts like inflammatory cells, leukocytes etc which is characteristic of the sputum sampling. These artifact regions are manually removed so that the remaining dataset consists of only nuclear regions. The entire sequence of preprocessing is shown in Figure. 3.

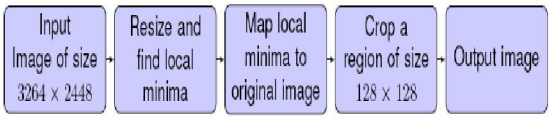

Figure 3: Block diagram of the preprocessing system

3.3 Segmentation

For segmentation we use 2 clustering techniques namely K-means and Fuzzy C-means on various color spaces such as HSV, CIELAB, CIEXYy and CIELUV. In the following section, we detail the clustering algorithms, the different types of color-space conversions used in our work

3.3.1 Clustering Techniques

K-means Clustering: K-means is an unsupervised clustering technique in which m data points with n dimension is grouped into k separate groups, $S_i, i = 1, \cdots, k$ [30]

$$\arg\min_{S} \sum_{i=1}^{k} \sum_{x_j \in S_i} \|x_j - \mu_i\|^2 \quad (1)$$

The grouping is done by minimizing the distance between data point and the centroid of the corresponding cluster to which it falls to. X_j the data point, μ_i the centroid of the i^{th} cluster, $\|\cdot\|^2$ is the l2 norm of a vector. The algorithm is run multiple times so that no more change to the data point happens. For this paper, k=2 is chosen, one for foreground and the other for background.

b) Fuzzy C-means Clustering

The K-means clustering assigns distinctly one group to each data point. In many applications, especially medical application, it may not be clear to which group a particular point belongs. In Fuzzy C-means a membership value is assigned to the data point for each cluster. A data point near the center of cluster has a high membership value to that particular cluster than a point near the edge of the cluster. The objective function is as follows

$$E = \sum_{j=1}^{c} \sum_{i=1}^{N} \mu_{ij}^{k} \|x_i - c_j\|^2 \quad (2)$$

μ_{ij} is the fuzzy membership of the data point x_i, c_j is the centroid, k is the constant defining fuzzyness of the cluster. After each iteration the membership function and cluster centroid is updated as

$$\mu_{ij} = \frac{1}{\sum_{m=1}^{C} \left(\frac{\|x_j - c_i\|}{\|x_j - c_m\|^{2/(k-1)}} \right)} \quad (3)$$

$$C_i = \frac{\sum_{j=1}^{N} \mu_{ij}^{k} x_j}{\sum_{j=1}^{N} \mu_{ij}^{k}} \quad (4)$$

3.3.2 Color Space Conversion

The RGB image contains pixel values which are highly correlated, so processing it directly results in redundant information processing. To uncorrelate this data we use other color spaces like HSV, LUV, LAB and xyY. Various conversion techniques used in this work are presented below.

a) RGB to HSV

The input RGB image is normalized before converting to HSV color space image using the following method [31].

$$N = max(R, G, B) \quad (5)$$

$$n = min(R, G, B) \quad (6)$$

Let, $r = \frac{N - R}{N - n}; g = \frac{N - G}{N - n}; b = \frac{N - B}{N - n};$ (7)

Value is $V = max(R, G, B)$ (8)

Saturation is $S = \frac{N - n}{n}$ (9)

Hue is

$$\begin{aligned} H &= \frac{\pi}{3}(b - g), \text{ if } R = N \\ &= \frac{\pi}{3}(2 + r - g), \text{ if } G = N \\ &= \frac{\pi}{3}(4 + g - r), \text{ if } B = N \end{aligned} \quad (10)$$

Normalized hue is $H = \frac{H}{2\pi}$ (11)

b) RGB to CIELAB

CIELAB color space is derived from CIEXYZ color space. In CIEXYZ all visible colors

are represented using only positive values. The color conversion matrix is as,

$$\begin{bmatrix} R \\ G \\ B \end{bmatrix} = \begin{bmatrix} 3.240479 & -1.53715 & -0.498535 \\ -0.969256 & 1.875992 & 0.041556 \\ 0.055648 & -0.204043 & 1.057311 \end{bmatrix} \times \begin{bmatrix} X \\ Y \\ Z \end{bmatrix} \quad \textbf{(12)}$$

The CIELAB color components are given by

$$A = 500\left[h\left(\frac{X}{X_w}\right) - h\left(\frac{Y}{Y_w}\right)\right] \quad (13)$$

$$B = 200\left[h\left(\frac{Y}{Y_w}\right) - h\left(\frac{Z}{Z_w}\right)\right] \quad (14)$$

$$h(q) = \sqrt[3]{q}, \text{, if } q > 0.008856$$
$$= 7.787q + 16/116, \text{if } q \leq 0.008856 \quad (15)$$

Where X_w, Y_w and Z_w are the white tristimulus values of a perfectly reflecting diffuser under CIE standard D65 illumination [32].

c) XYZ to xyY

CIExyY is derived from CIEXYZ color space. The conversion is as follows

$$x = \frac{X}{X+Y+Z} \quad (16)$$

$$y = \frac{Y}{X+Y+Z} \quad (17)$$

$$Y = Y \quad (18)$$

d) CIEXYZ to CIELUV

LUV color space is derived from XYZ color space. The conversion is as follows

$$u' = \frac{4X}{X+15Y+3Z} \quad (19)$$

$$v' = \frac{9Y}{X+15Y+3Z} \quad (20)$$

$$L^* = 116\left(\frac{Y}{Y_w}\right)^{\frac{1}{3}}, \text{ if } \frac{Y}{Y_w} > \left(\frac{6}{29}\right)^3$$
$$= \left(\frac{29}{3}\right)^3\left(\frac{Y}{Y_w}\right), \text{ if } \frac{Y}{Y_w} \leq \left(\frac{6}{29}\right)^3 \quad (21)$$

$$u^* = 13L^*(u' - u'_w) \quad (22)$$

$$v^* = 13L^*(v' - v'_w) \quad (23)$$

3.3.3 Segmentation procedure

The identified nuclear regions are fed to the segmentation module. The staining of sputum cytology images generally does not give uniform color distribution. So identifying nuclear regions based on one particular color may not give good segmentation result. The information content in RGB color space is highly correlated and to uncorrelate it, various color spaces is used. Some information may be discernable in one color space may not be quiet as well distinguished in another color space. A novel method of combining various color spaces is used in the segmentation module. The technique is a generalization of the method used by Issac et al [31] where K-means clustering is done on LAB color space. In this method the input image is first converted to LAB, LUV, HSV and xyY color spaces. Paired combinations of layers within these color spaces are then taken and K-mean/FCM clustering is performed upon them. The 20 combination consists of LAB layer L-A, LAB layer A-B, LAB layer L-B, HSV layer H-S, HSV layer S-V, HSV layer H-V, xyY layer x-y, xyY layer y-Y, xyY layer x-Y , LUV layer L-U and HSV layer S only. The different combination gives a different result for the segmentation using K-means and FCM algorithm

The K-means and FCM algorithms give different labels for nuclear region in different images. So it is required to find the correct label for the nuclei region alone. The image cropping done in the preprocessing stage ensures that nuclear region is present near the middle of the image. So 100 pixels at the center of the image is taken and the median value is found. The label of the median is considered as the label for the nucleus. Then morphological closing followed by opening is performed to join small unconnected regions in the image using a 3 x 3 square structuring element. Then hole filling is done to remove holes inside nucleus region. From the resulting image the object with largest area is separated. This region gives the result of segmentation. This process is done on all the 20 results. Finally the best segmentation result has to be chosen. For this a weight value is given for each of the segmentation result. This is given by

$$weight = \frac{area}{convex\ area} - \frac{pixel\ in\ border}{total\ border} \quad \textbf{(24)}$$

The criterion for giving the first part is that most of the nuclear regions are of elliptical shape or shapes closer to that. So the ratio of area to convex area gives higher weight to convex shapes than concave shapes. The K-means and Fuzzy C-means algorithm are not guaranteed to find two separate regions sometimes only one region is returned i.e., the entire image itself giving maximum weight to such an image. So this condition has to be eliminated, for this a penalty term is added. The second term gives a penalty depending on the number of pixels that are clustered touches the boundary of the image. If no pixel is touching the border then the penalty is zero otherwise a positive value. If an erroneous clustering result comes to cover the entire image, the penalty value become 1 and so also the first term, giving 0 value effectively. Thus the image is eliminated from further analysis being the lowest weight value. From the 20 segmented results one with maximum weight is taken as the final segmented result. The various step of segmentation are shown in Figure 4.

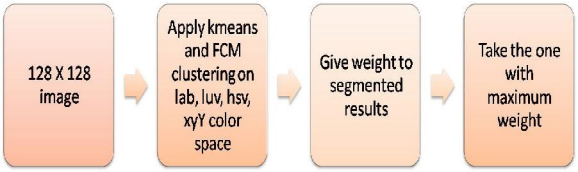

Figure 4. The steps of segmentation algorithm

3.4 Feature Extraction using Scale Space

This is the most crucial part of the system where the scale space features are extracted. Scale space deals with the observation or study of image at various scales. It is about describing an image according to the size/scale of objects present in the image. In this paper we are using scale space catastrophe points as features. Catastrophe points or top points were successfully used for image matching and reconstruction [34]. In this work we are using catastrophe points for extracting features from the nuclear region.

3.4.1 Scale Space

In the physical world every object has the corresponding property which we observe occur at certain scale of observation only. That is to know about an object we should analyze it at that particular scale which is meaningful to the under study. This forms the basis of scale space theory [35]. Convolving the image with a Gaussian kernel gives the linear scale space representation [36]. Linear scale space was the unique kernel which satisfies the following axioms [37]

- linearity, i.e., there is no knowledge of any kind
- spatial scale invariance, i.e., all objects whether small or large are treated equally
- spatial homogeneity, i.e., no preference is given to any particular location
- spatial isotropy, i.e., all orientations are treated equally

It was shown that if separability is not a criterion then there exist infinite linear scale spaces [38]. In this analysis the linear Gaussian scale space is considered. The scale space images are obtained by the convolution of an image with a Gaussian kernel of varying size. ie L : R2 →R.

$$L(x,\sigma) = g(x,\sigma) \otimes L(x) \quad (25)$$

Where L(x; 0) = L(x), is the original image.

$$g(x,\sigma) = \frac{1}{(2\pi\sigma^2)^{D/2}} e^{-\left(\frac{x_1^2+\ldots+x_D^2}{2\sigma^2}\right)} \quad (26)$$

D is the dimensionality in this case 2 and σ the standard deviation of Gaussian kernel

3.4.2 Deep Structure

The scale space stack is generated and stored for further analysis. There are certain interesting events which happen in the scale space. This can be analyzed only by observing the scale space stack as a whole i.e. both along spatial and scale dimensions and this is termed as deep structure [36]. One of the most important features is the automatic detection of the scale of singularities like edges, blobs etc. [39]. In general deep structure analysis shows that the singularities decrease as we move up the scale space stack [40]. This is due to the annihilation and creation of singularities depending on the scale of observation. This analysis leads to the well known catastrophe theory [41].

3.4.3 Catastrophe Theory

Observing singularities alone in the scale space stack gives a basic idea of the image structure. Analyzing the singularity leads to the catastrophe points where major change to scale space image structure occurs [40]. Consider a smooth function (in C^{α}) f with n states and m control parameters, $f(x_1 \ldots, x_n; c_1 \ldots, c_m) \in C^{\alpha}(R^{n+m};R)$. The points in f can be classified in 3 ways

- Regular : $\exists l \in [1 \ldots n]$ such that $\frac{\partial f}{\partial x_l} \neq 0$
- Morse Singularity: $\frac{\partial f}{\partial x_i} = 0$ and Det $\left(\frac{\partial f}{\partial x_i \partial x_j}\right) \neq 0$
- Catastrophe: $\frac{\partial f}{\partial x_i} = 0$ and Det $\left(\frac{\partial f}{\partial x_i \partial x_j}\right) = 0$

For a 2D image state corresponds to spatial co-ordinates (n = 2) and control parameter corresponds to scale (m = 1).

3.4.4 Finding catastrophe points

Maxima, minima and saddle points are found on all the scales using Blom's method [47]. Here hexagonal neighborhood are considered for processing. Even rows in rectangular grid are shifted half pixel to the right to form the hexagonal grid. In practice this turns out to be taking the 8 nearest neighbors and discarding top right and bottom right neighbors for even rows and discarding top left and

bottom left elements for odd rows [33] as shown in Figure. 5.

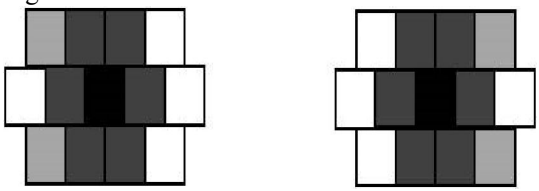

Figure 5: Center pixel (black), hex neighborhood (medium gray), excluded pixels (light gray) from 8 neighborhood for odd (left) and even (right).

For these 6 neighbors the sign of the difference with center pixel is found. This leads to 4 cases [33] as shown in Figure. 6

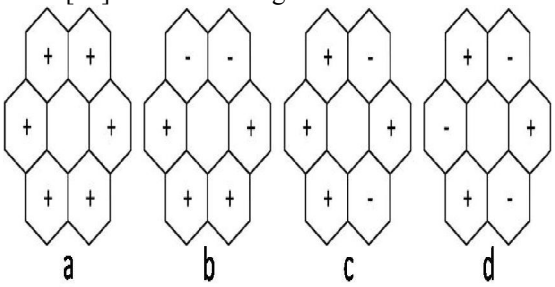

Figure 6: a) extremum b) regular c) saddle d) monkey saddle

* No sign change, the given point is an extrema
* Two sign changes, the point is a regular point
* Four sign changes, the point is a saddle
* Six sign changes, the point is a monkey saddle

The maxima, minima and saddle points found are arranged over all the scales. At each level these critical points are connected to the level above it using nearest neighbor approach. The linking is done at all the scales. Whenever the critical points reach their annihilation catastrophe they cease to exist in the subsequent higher scales. The level at which this happens is identified and marked as the catastrophe level of that critical point. The saddle-maxima and saddle minima catastrophe is found using nearest neighbor linking. The experimental results show that the number of catastrophe points is more for malignant cases than for benign cases. The block diagram for the overall feature extraction system is given in the Figure 7.

Scale space stack is generated for 32 scales ranging from e^1 to e^3. The intermediate scales are chosen in such a way that the ratio between any two successive scales is the same [39]. The count for catastrophe points, both saddle-maxima and saddle-minima, occurring for each scale is taken and the feature vector is generated thus producing a size of 64 dimensional vector.

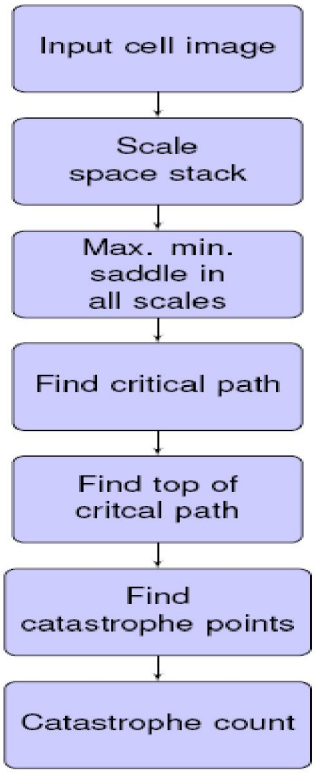

Figure 7: Block diagram of feature extraction system

3.4.5 Feature Extraction

3.5 Classification

The classifier forms the final part of the system. Studies on lung cancer detection have shown that SVM classifier yielded good results in terms of accuracy [42]. Our training set consists of 100 cells from both benign and malignant cases. The classification of the selected cells was done manually by expert cytopathologist. The testing sample consists of 768 benign and 270 malignant cells. We have used the non linear Radial Basis Function (RBF) kernel for SVM. The accuracy of the classifier is as shown in Table 1.

Performance Parameter	No. of images
True Positive	112
True Negative	704
False Positive	64
False Negative	158
Accuracy	78.61%

Table 1: Accuracy using SVM RBF kernel

4 Results and Discussion

The cellular region from input high resolution image 3264 X 2448 is cropped out and is shown in Figure. 8. Majority of the cellular regions

were detected and fed to the subsequent segmentation stage. In this stage the exact region of nucleus is delineated. Cropped cellular regions for benign and malignant cells are shown in Figure. 9. The cropped cellular region is subsequently processed in the segmentation module where the exact nuclear region is obtained. For segmentation of nuclear region, 20 results are obtained using various combinations of color spaces and clustering using FCM and K-means from which the best is chosen. The segmentation result along with clustering technique, color space, color channels used and corresponding weight is shown in Figure. 10 The best segmentation result follows to the feature extraction stage where the catastrophe points are extracted. Maxima, minima and saddle points are detected from the images in the scale space stack that are shown in Figure 11. Experimental results for two sample benign and malignant cases are shown in Figure 12, where the number of catastrophe points is more for malignant cases than for benign cases. This helps us to classify benign and malignant cells from the lung glandular cells.

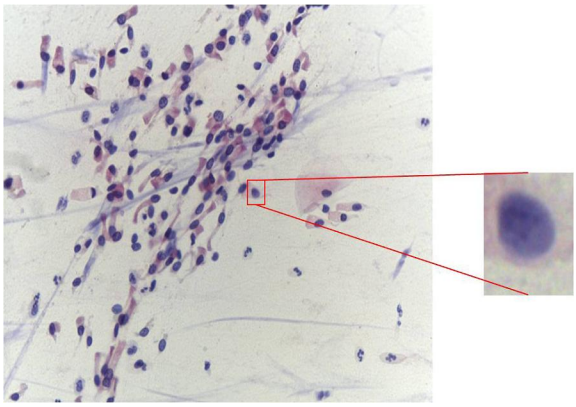

Figure 8: Cropped nucleus from the input image

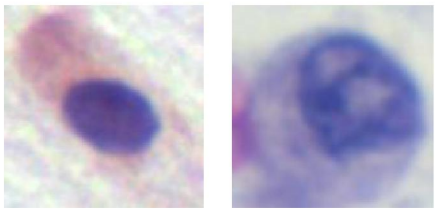

Figure 9: Cropped image a) benign cell b) malignant cell

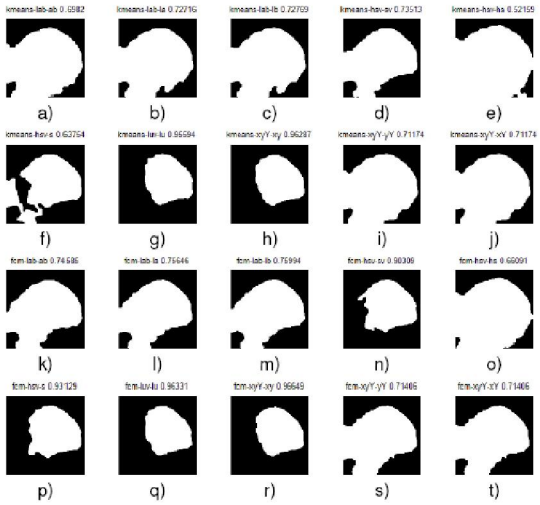

Figure 10: Segmentation results for benign cell

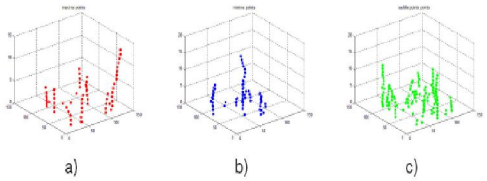

Figure 11: a) Maxima b) Minima c) Saddle for various scales

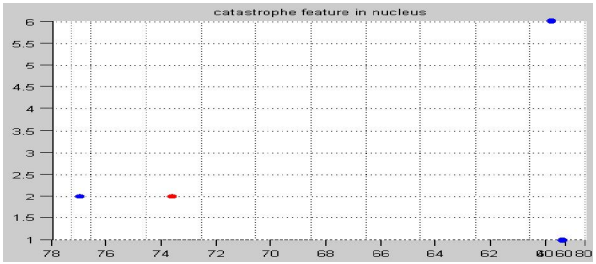

Begnin case 1

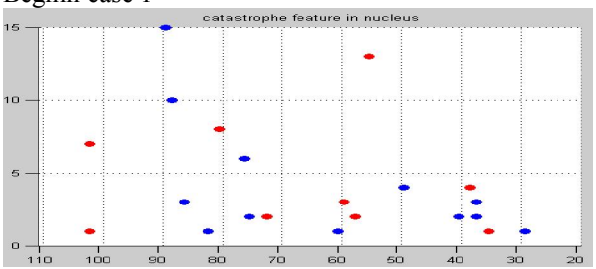

Malignant case 1

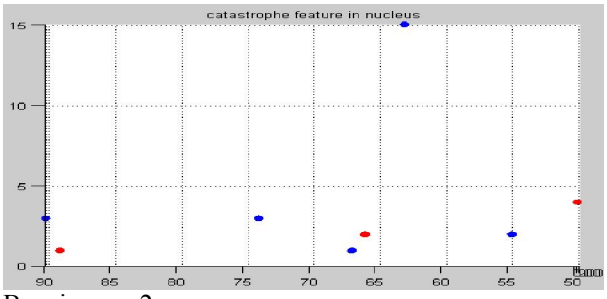

Begnin case 2

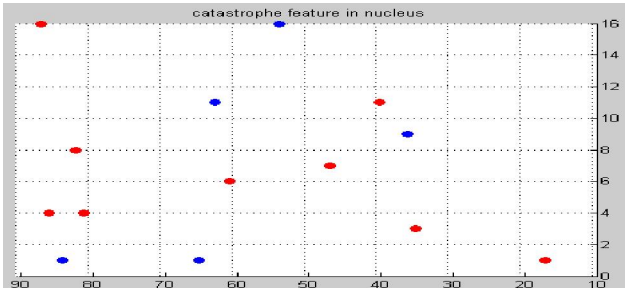

Malignant case 2

Figure 12. The experimental results for two sample benign and malignant cases with catastrophe points

5 Conclusion and Future work

In this paper, we have presented a novel method for lung glandular cell segmentation using multiple color spaces and two clustering techniques namely FCM and C-Means. Catastrophe points are used as features and SVM is used as classifier for the purpose. The system successfully identifies the cellular regions as benign or malignant when the cropped region is fed. As future work we plan to improve the accuracy by adding more features and a fully automated system which will automatically remove artifacts.

ACKNOWLEDGEMENTS

As authors, we are very much grateful to Dr. C Shunmuga Velayutham , Dept. of Computer Science and Engineering, Amrita Viswa Vidyapeetham, Coimbatore India , for his valuable support throughout our work. We would also like to extend our sincere thanks to Nimi G K of Pathology lab, Regional Cancer Center, Thiruvananthapuram, India for helping us in gathering the dataset.

6. References

[1] J. P. Thiran; B. Macq, Morphological feature extraction for the classification of digital images of cancerous tissue, IEEE Transactions on Biomedical Engineering, Publication Year: 1996, Vol. 43, Page(s): 1011-1020

[2] R. F. Walker; P. Jackway; B. Lovell, & I. D. Longstaff, Classification of cervical cell nuclei using morphological segmentation and textural feature extraction, Proceedings of the 1994 Second Australian and New Zealand Conference on Intelligent Information Systems. Publication Year: 1994, Page(s): 297-301

[3] H. Wu; J. Gil; J. Barba, Optimal segmentation of cell images, IEEE Proceedings -Vision, Image, and Signal Processing. Publication Year: 1998, Vol. 145, No. 1, Page(s): 50-56

[4] F. Schnorrenberg; C. S. Pattichis; K. C. Kyriacou,; C. N. Schizas, Computer-aided detection of breast cancer nuclei, IEEE Transactions on Information Technology in Biomedicine. Publication Year: 1997 , Vol 1, Page(s): 128-140

[5] T.Tanaka; T. Joke; T. Oka, Cell nucleus segmentation of skin tumor using image processing. Proceedings of the 23rd Annual International Conference of the IEEE Engineering in Medicine and Biology Society. Publication Year: 2001, Vol 3, Page(s): 2716-2719 ,

[6] M. Sammouda; N. Niki; T. Niki; N. Yamaguchi, Analysis of color images of tissues derived from patients with adenocarcinoma of the lung. IEEE Proceedings of 2000 International Conference on Image Processing. Publication Year: 2000, Vol 1, Page(s): 192-195

[7] C. Wittke; J. Mayer; F. Schweiggert, On the classification of prostate carcinoma with methods from spatial statistics. IEEE Transactions on Information Technology in Biomedicine. Publication Year: 2007, Vol 11, Page(s): 406-414

[8] V. Meas-Yedid; S. Tilie; J. C. Olivo-Marin, Color image segmentation based on markov random field clustering for histological image analysis. Proceedings 16th International Conference on Pattern Recognition. Publication Year: 2002 Vol 1, Page(s): 796-799

[9] G. Begelman; E. Gur; E. Rivlin; M. Rudzsky; Z. Zalevsky, Cell nuclei segmentation using fuzzy logic engine. IEEE International Conference on Image Processing. Publication Year: 2004, Vol 5, Page(s): 2937- 2940

[10] M. Hu; X. Ping; Y. Ding, Automated cell nucleus segmentation using improved snake. International Conference on Image Processing. Publication Year: 2004, Vol 4, Page(s): 2737-2740

[11] P. Phukpattaranont; P. Boonyaphiphat:, Segmentation of cancer cells in microscopic images using neural network and mathematical morphology. IEEE International Joint Conference SICE-ICASE. Publication Year: 2006, Page(s): 2312–2315.

[12] B. Ko, M. Seo; J. Nam, Microscopic image segmentation for the clinical support system. IEEE Computer Graphics, Imaging and Visualisation. Publication Year: 2007 Page(s): 489-494
[13] G. Palacios; J. R. Beltran, Cell nuclei segmentation combining multiresolution analysis, clustering methods and colour spaces. IEEE International Conference on Machine Vision and Image Processing. Publication Year: 2007, Page(s): 91-97
[14] F. Taher; R. Sammouda, Lung cancer detection by using artificial neural network and fuzzy clustering methods. IEEE GCC conference and Exhibition. Publication Year: 2011, Page(s): 295-298
[15] M. E. Plissiti; C. Nikou; A. Charchanti, Automated detection of cell nuclei in pap smear images using morphological reconstruction and clustering. IEEE Transactions on Information Technology in Biomedicine. Publication Year: 2011, Vol. 15, Page(s): 233-241
[16] W. Wang; J. A. Ozolek; D. Slepcev,; A. B. Lee; C. Chen; G. K. Rohde, An optimal transportation approach for nuclear Structure-Based pathology. IEEE Transactions on Medical Imaging. Publication Year: 2011, Vol. 30, Page(s): 621-631
[17] Z. Huang; D. Liu, Segmentation of color image using EM algorithm in HSV color space. IEEE International Conference on Information Acquisition. Publication Year: 2007, Page(s): 316–319
[18] T. Chen; Y. Chen; S. Chien, Fast image segmentation based on KMeans clustering with histograms in HSV color space. IEEE 10th Workshop on Multimedia Signal Processing. Publication Year: 2008, Page(s):322-325
[19] G. Zhao; S. Wang; T. Wang; J. Chen, HSV color space and face detection based objectionable image detecting. Second International Conference on Future Generation Communication and Networking Symposia. Publication Year: 2008, Vol. 3, Page(s): 107-110
[20] Y. Lu; W. Gao; J. Liu, Color matching for colored fiber blends based on the fuzzy c-mean cluster in HSV color space. Seventh IEEE International Conference on Fuzzy Systems and Knowledge Discovery. Publication Year: 2010 Vol. 1, Page(s): 452-455
[21] V. Anari; P. Mahzouni; R. Amirfattahi, Automatic extraction of positive cells in pathology images of meningioma based on the maximal entropy principle and HSV color space. 6th Iranian conference on Machine Vision and Image Processing. Publication Year: 2010, Page(s): 1-4
[22] M. H. Asmare; V. S. Asirvadam; L. Iznita, Color space selection for color image enhancement applications. IEEE International Conference on Signal Acquisition and Processing. Publication Year: 2009, Page(s): 208-212
[23] H. Rami; M. Hamri; L. Masmoudi, Hybrid color space and support vector machines for classification. IEEE International Conference on Multimedia Computing and Systems, Publication Year: 2009, Page(s): 484-487
[24] N. M. Kwok; Q. P. Ha; G. Fang, Effect of color space on color image segmentation. 2nd IEEE International Congress on Image and Signal Processing. Publication Year: 2009, Page(s): 1-5
[25] Y. Pu; X. Wei; Y. Su; Z. Zhao; W. Qian,; D. Xu, Implementation and research of multi-method color transfer algorithms in different color spaces. IEEE 2010 International Conference on Machine Vision and Human-Machine Interface. Publication Year: 2010, Page(s): 713-717
[26] Z. Yux; W. Yuhua; L. Haibo, A fuzzy c-means clustering based on hybrid color space. IEEE International Conference on Electrical and Control Engineering. Publication Year: 2010, Page(s): 4605-4607
[27] D. Hang; L. Xi, The color components' computing on different color spaces for image segmentation of hematocyte. IEEE International Symposium on Intelligence Information Processing and Trusted Computing. Publication Year: 2010, Page(s): 75–78
[28] S. Chen; C. Liu, Fast eye detection using different color spaces. IEEE International Conference on Systems, Man, and Cybernetics. Publication Year: 2011, Page(s): 521-526
[29] L. Bradbury; J. W. Wan, A spectral k-means approach to brightfield cell image segmentation. Annual International Conference of the IEEE Engineering in Medicine and Biology Society. Publication Year: 2010, Page(s): 4748–4751
[30] J. Macqueen, Some methods of classification and analysis of multivariate observations. Proceedings of the Fifth Berkeley Symposium on Mathematical Statistics and Probability. Publication Year: 1967, Page(s):281–297
[31] S. Issac Niwas; P. Palanisamy; R. Chibbar; W. J. Zhang, An expert support system for breast cancer diagnosis using color wavelet features. Journal of Medical Systems. Publication Year: 2011, Page(s): 1-12
[32] R. C. Gonzalez; R. E. Woods, Digital Image Processing. Prentice Hall, 2007

[33] A. Kuijper, On detecting all saddle points in 2D images. Pattern Recognition Letters. Publication Year: 2004, Vol. 25, Page(s): 1665-1672

[34] R. Kimmel; N. A. Sochen; J. Weickert; D. Hutchison; T. Kanade; J. Kittler; J. M. Kleinberg; F. Mattern; J. C. Mitchell; M. Naor; O. Nierstrasz; C. Pandu Rangan; B. Steffen; M. Sudan; D. Terzopoulos; D. Tygar; M. Y. Vardi; G. Weikum (eds), Scale Space and PDE Methods in Computer Vision. Springer Berlin Heidelberg, Berlin, Heidelberg.Vol. 3459, Page(s): 431–442

[35] T. Lindeberg; Scale-space theory: A basic tool for analyzing structures at different scales. Journal of applied statistics. Publication Year: 1994, Page(s): 224-270

[36] J. Koenderink, The structure of images. Biological Cybernetics. Vol. 50. No. 3, Page(s): 363 – 370

[37] L.M.J. Florack; B.M.T.H. Romeny; j.Koenderink; M.Vigergevef; Linear scale-Space. Journal Mathematics Imaging. Publication Year: 1994, Vol. 4. No. 4. Page(s): 325 – 351

[38] R. Duits; L. Florack; J. Degraft; B. Ter haar Romeny; On the axioms of scale space theory, Journal mathematics Imaging. Publication year: 2004. Vol. 20. No.3, Page(s): 267 – 298

[39] T. Lindeberg, Feature detection with automatic Scale selection. International journal computer Vision. Publication year: 1998, Vol. 30. No.2, Page(s): 79 – 116

[40] B.M.H. Romemy, Front-end vision and multi Scale Image Analysis, Multiscale computer vision Theory and Applications mathematics. Springer Publication year: 2003

[41] L.Florack; A.Kuijper, The Topological structure Of scale-space images, Publication year: 1998

[42] K. kancherla; s.Mukkamala, Feature selection For Lung cancer detection using SVM based Recursive feature elimination method, Springer Berilin/Heidelberg, Publication year: 2012

[43] K. Rodenacker; E. Bengtsson, A feature set for cytometry on digitized microscopic images. Analytical cellular Pathology, Publication Year: 2003, Vol 25. No. 1, Page(s): 1 – 36

[44] R.S. Hode; G. Saccommama; K. Schroiber; D.Decker; L.G.Koss, Automated sputum Screening With papnet system: A study of 122 cases, Human Pathology, Publication year: 1996 Vol. 27. No. 7. Page(s) 656 – 659

[45] S. Doyle; M. Hwang; K. Shah; A. Madabhusi; J. Tomaszeweski, Automated grading of Prostate Cancer using architectural and textural image features, Proceeding 4th IEEE International Symposium on Biomedical Imaging: From nano to Macro, Arlington Apr 12 - 14, Page(s): 1248 – 1287

[46] S.I. Niwas, P. Paliniswamy; W.J. Zhang; N.A.M. Isa; R. Chibbar, Log-gabor wavelets based breast Carcinoma classification using least square Support vector machine, Proceeding IEEE International Conference Imaging Systems and Techniques Penang, May 2011,Page(s): 219 – 223

[47] J. Blom, Topological and Geometrical aspects of Image structure, Ph.d Thesis, Utrecht university 1992.

6/4/2013